JOURNAL OF MATERIALS SCIENCE **40** (2005) 5839–5844

Strain-energy based homogenisation of two- and three-dimensional hyperelastic solid foams

SERKAN DEMIRAY, WILFRIED BECKER
TU Darmstadt, Institut für Mechanik, Hochschulstr. 1, 64289 Darmstadt, Germany
E-mail: demiray@mechanik.tu-darmstadt.de
E-mail: becker@mechanik.tu-darmstadt.de

JÖRG HOHE
Fraunhofer-Institut für Werkstoffmechanik (IWM), Wöhlerstr. 11, 79108 Freiburg/Brsg., Germany
E-mail: hohe@iwm.fhg.de

A possible classification of cellular solids can be made based on the dimension into honeycombs and foams. In numerical simulations 2D models that are employed primarily to study honeycombs can also be used to model open-cell foams. Thereby, a loss of information regarding the 3D connectivity of the microstructure is involved. To answer the question how the missing third dimension in 2D models affects the overall properties, spatially periodic 2D and 3D model foams are adopted. From the point of homogenisation, a strain-energy based scheme is used for adequately determining the effective mechanical properties at large strains. The key idea behind this method is to use directly the equivalence condition between the meso-strain energy and the macro-strain energy. In a first step a representative volume element with the given microstructure and a corresponding volume element containing the effective medium are subjected to equivalent states of deformation. Subsequently, the macroscopic stress-strain relationships are determined by volume-averaging of the stored strain energy. The results of some fundamental loading cases indicate that both model foams represent the deformation characteristics of hyperelastic solid foams like localized bending and elastic buckling. In addition, the development of anisotropy due to microstructural changes at large strains can be traced with both model foams. Nevertheless, the different cell morphology affects the stress-strain curves in a quantitative manner.

1. Introduction

Cellular solids like polymeric or metallic foams are advanced materials whose microstructure can be tailored by appropriate control of the production process to a certain degree. In addition, the high porosity of the microstructure makes these materials suitable for lightweight constructions. Besides their application for structural components, open-celled foams can be also used as heat exchangers or catalytic converters. Owing to their pore structure, these materials differ significantly from conventional materials, especially in compression loading.

Apart from the properties of the bulk material the foam is made of, the cellular microstructure has to been taken into account for if we want to predict its overall properties. The microstructural description of a foam comprises mainly information about the cell morphology and cell connectivity.

The first contributions to foam mechanics were made by Gent and Thomas [1] as well as by Patel and Finnie [2]. Closed-form analytically performed studies by Gibson and Ashby [3] on simple micromechanical models yield scaling rules for the effective Young's modulus and Poisson's ratio. The textbook of Gibson and Ashby [3] gives a good review on foam mechanics.

Warren and Kraynik [4] examined a regular honeycomb microstructure in the small strain regime. Owing to its six-fold symmetry, the hexagonal honeycomb model exhibits isotropic mechanical behaviour [5]. From the point of modeling, the honeycomb microstructure is suitable for physical reasons since the hexagons are space-filling polygons partitioning a plane in equal cells with minimal material input.

The three-dimensional counterpart of the hexagon can be derived from the Kelvin foam. The Kelvin foam which consists originally of closed cells with slightly

0022-2461
DOI: 10.1007/s10853-005-5017-6

curved cell walls can be approximated by a bcc-lattice of tetrakaidecahedral cells. In this study, the three-dimensional model is based on Kelvin's structure but the tetrakaidecahedral cells do not have closed faces in order to model open-cell foams. Hereby, a tetrakaidecahedron is a 14-sided polyhedron, containing six squares and eight hexagons. Warren and Kraynik [6] were the first determining the linear elastic properties of this microstructure. Zhu and his colleagues [7] derived analytic formulae for the overall linear elastic properties of the tetrakaidecahedron. In the comparative study of Grenestedt [8] different cellular periodic models were evaluated in the small strain regime.

One of the early papers on the non-linear behaviour of the regular Kelvin foam was by Dementjew and Tarakanov [9], whereby they only considered cell wall bending. Zhu *et al.* [10] examined the Kelvin foam under high-strain compression. The model used by Warren and Kraynik consists of a tetrahedral element. Wang and Cuitiño [11] analyzed the deformation evolution of a similar model at the mesoscopical level. Other modeling approaches are based on Voronoi tesselation (Zhu *et al.* [12]). However, by this technique irregular foam models are preferrably generated.

Aim of the present study is to examine the influence of the missing third dimension in 2D models on the overall mechanical behaviour of hyperelastic solid foams at large strains. Therefore, we focus on idealized periodic model foams although real foams exhibit a complex microstructural geometry. For the numerical homgenisation a strain energy based scheme (see [13, 14]) is adopted. This concept assumes that a representative volume element of the given microstructure and a volume element of the effective medium are mechanically equivalent if both volume elements hold the same amount of strain energy for the same effective macroscopic deformation. The finite deformations of both volume elements on the macroscopic level are linked via the volume average of the deformation gradient. Finally, for several fundamental loading situations the macroscopic stress-strain curves are compared and the relation between microstructural changes and macroscopic behaviour is demonstrated.

2. Homogenisation scheme

The process of homogenisation is depicted by means of Fig. 1. A hyperelastic cellular body in the domain Ω is loaded with surface tractions $t_i = \sigma_{ij} n_i$ and prescribed displacements u_i. We want to replace the complex microstructure in the vicinity of a material point X_i by a macroscopically equivalent medium which is ideally homogeneous. Provided that the cellular solid behaves statistically homogeneous at the macro level, the material point can be chosen arbitrarily and the space around this point is denoted as a representative volume element (RVE). Because of the periodic composition of the microstructures, considered in this study, the representative volume element is given by the smallest repeating unit of the infinite lattice. From the available homogenisation schemes proposed in literature for determining the overall mechanical properties of cellular and porous material, a strain energy based concept is adopted. The main advantage of this homogenisation procedure is that large deformation can be incorporated in a natural manner and for hyperelastic foams the overall stress- strain relationship corresponds to the constitutive equation on the meso level.

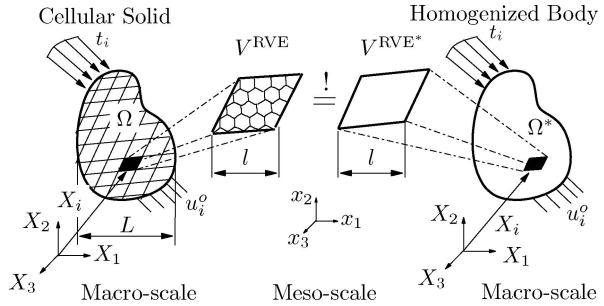

Figure 1 Homogenisation process of a periodic solid.

The key idea behind the proposed homogenisation framework can be described as follows: We consider a representative volume element containing the given cellular microstructure and a identical RVE filled with an ideally homogeneous effective medium with unknown properties. If both volume elements are subjected to macroscopically equivalent states of deformation, the same amount of strain energy has to be stored in both RVE for equivalent mechanical behaviour on the maco level. The condition of equal states of deformation can be expressed by

$$\bar{F}_{ij} = \frac{1}{V^{\mathrm{RVE}}} \int_{\Omega^{\mathrm{RVE}}} F_{ij}\, dV \stackrel{!}{=} \frac{1}{V^{\mathrm{RVE}}} \int_{\Omega^{\mathrm{RVE}}} F^*_{ij}\, dV = \bar{F}^*_{ij} \tag{1}$$

where F_{ij} denotes the components of the deformation gradient tensor. Furthermore, quantities that are marked by an asterisk refer to the effective medium.

The assumption of equivalent strain energies on the meso and macro level is given by

$$\bar{w} = \frac{1}{V^{\mathrm{RVE}}} \int_{\Omega^{\mathrm{RVE}}} w\, dV \stackrel{!}{=} \frac{1}{V^{\mathrm{RVE}}} \int_{\Omega^{\mathrm{RVE}}} w^*_{ij}\, dV = \bar{w}^*_{ij}. \tag{2}$$

Therein, w and w^* denote the strain energy densities in RVE and RVE*, respectively. In addition to the deformation gradient in Equation 1, the Green-Lagrange strain tensor is introduced as strain measure by

$$\bar{\gamma}_{ij} = \frac{1}{2}(F_{ki} F_{kj} - \delta_{ij}) \tag{3}$$

where δ_{ij} is the Kronecker delta tensor.

Since large elastic deformations of the model foams are taken into account, a hyperelastic material model is assumed on the meso level. By differentiation of the strain energy with respect to the Green-Lagrange strain tensor, the components of the second Piola-Kirchhoff stress tensor are obtained:

$$\bar{\tau}_{ij} = \frac{\partial \bar{w}}{\partial \bar{\gamma}_{ij}} \quad . \tag{4}$$

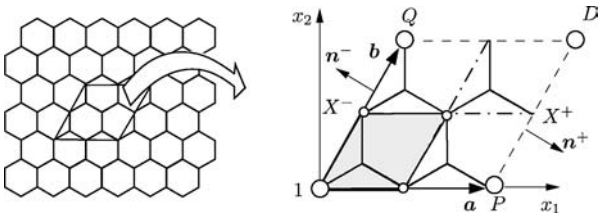

Figure 2 Hexagonal lattice and RVE consisting of 2 × 2basic cells.

As an alternative stress measure, Cauchy stresses that refer to the current configuration of the RVE are introduced. From the 2nd Piola Kirchhoff stresses, the Cauchy stress tensor can be evaluated by

$$\bar{\sigma}_{ij} = \frac{1}{\bar{J}} \bar{F}_{ik} \bar{F}_{jl} \bar{\tau}_{kl}, \quad \bar{J} = \det \bar{\boldsymbol{F}} \tag{5}$$

where $\bar{J}$ is the determinant of the deformation gradient.

3. Mesoscopic modeling

3.1. Representative volume elements

Within the scope of a micromechanical approach, the concept of representative volume elements (RVE) is used in the present study. For both type of model foams the RVE has the shape of a parallelepiped spanned by vectors $\boldsymbol{a}$, $\boldsymbol{b}$ and $\boldsymbol{c}$. Due to the periodicity of the microstructures, a RVE can be made up of several basic cells. Hereby the term 'basic cell' denotes the smallest possible repeating unit. For loading cases without instability phenomena, one basic cell is sufficient to determine the overall stress-strain curves, otherwise $n = 2$ or more basic cells in each translation direction are required to capture the microstructure's deformation.

In Fig. 2 it is shown how a RVE for the 2D model can be generated. The vectors $\boldsymbol{a}$ and $\boldsymbol{b}$ span the RVE in the x_1, x_2-plane. A basic cell is composed of three cell walls meeting at a angle of 120°. The microgeometry of the 2D model foam is discretized using 4-node shell elements. In order to apply a plane strain state, all nodes are fixed in x_3-direction.

In Fig. 3a the 3D model foam consisting of $2 \times 2 \times 2$ basic cells is presented. With respect to the (x_1, x_2, x_3) coordinate system, the nodal points are given by $P\,(d, d, d)$, $Q\,(-d, d, d)$ and $R\,(0, 2d, 0)$, whereas in Fig. 3b the basic cell of the 3D model foam is shown. Again, a parallelepiped is cut from the bcc-lattice of tetrakaidecahedral cells. The basic cell within the 3D-RVE comprises 12 cell struts and 12 cell vertices. The struts of the microstructure are discretized using Timoshenko beam elements. The Plateau border cross-section observed in real polymeric foams is approximated with an equilateral triangle.

Because of the large elastic deformation that rubber-like materials can expericence, a hyperelastic material model of Mooney-Rivlin form is assumed on the cell wall level.

3.2. Boundary conditions and loading

It is assumed that the deformation of the RVE exhibits periodicity. Thus, two opposing planes $\Gamma^+$and Γ^- of the boundary with outward normals $\boldsymbol{n^+ = n^-}$ are supposed to deform in a compatible manner. Since the finite element method is used, discrete periodicity constraints are imposed for the surface nodes. To give an example, the periodicity conditions for the nodes X^+ and X^- in Fig. 2 read

$$\begin{matrix} u_i^{(+)} - u_i^{(P)} = u_i^{(-)} - u_i^{(1)} \\ \varphi_i^{(+)} \quad = \quad \varphi_i^{(-)} \end{matrix}, \quad i = 1, 2, 3 \tag{6}$$

with $u_i^{(\cdot)}$ denoting the displacements of the corresponding nodes and $\varphi_i^{(\cdot)}$ the respective rotation angles.

Applying periodicity constraints, the volume average of the deformation gradient (see Equation 1) can be expressed in terms of the displacements $u_i^{(P)}$, $u_i^{(Q)}$, and $u_i^{(R)}$

$$\bar{F}_{ij} = \frac{1}{V^{\mathrm{RVE}}} \left\{ u_i^{(P)} \boldsymbol{b} \times \boldsymbol{c} \cdot \mathbf{e}_j + u_i^{(Q)} \mathbf{c} \times \mathbf{a} \cdot \mathbf{e}_j \right. \\ \left. + u_i^{(R)} \mathbf{a} \times \mathbf{b} \cdot \mathbf{e}_j \right\} + \delta_{ij} \tag{7}$$

where $\boldsymbol{e}_j$ denotes the basic unit vector in x_j-direction. Hereby, the transformation of the volume integral to a surface integral yields:

$$\bar{F}_{ij} = \frac{1}{V^{\mathrm{RVE}}} \int\limits_{\partial \Omega^{\mathrm{RVE}}} u_i n_j + \delta_{ij} \quad . \tag{8}$$

For a prescribed macroscopic strain state the displacements $u_i^{(P)}$, $u_i^{(Q)}$, and $u_i^{(R)}$ of the master nodes are determined numerically by means of the Equations 3 and 7 in terms of the components $\bar{\gamma}_{ij}$ of the macroscopic Green-Lagrange strain tensor. In addition, node 1 is fixed to suppress rigid body translations of the RVE

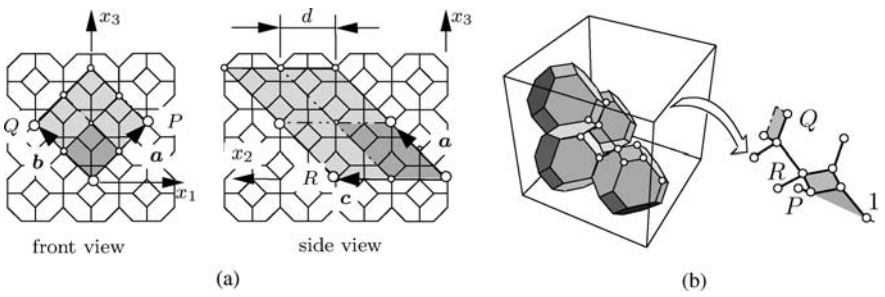

Figure 3 (a) Bcc-lattice of tetrakaidecahedral cells. (b) Basic cell.

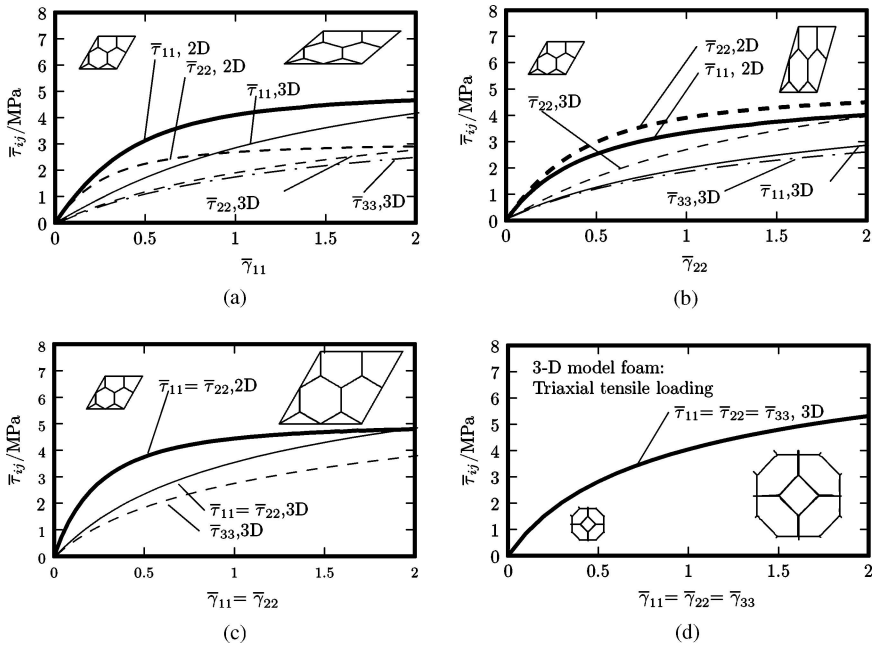

Figure 4 Effective stress-strain curves for uni- and multi-axial tensile deformation.

and a symmetric deformation gradient is assumed in order to eliminate rigid body rotations.

4. Numerical results and discussion

4.1. Uni- and multiaxial tensile deformation

In a first example the foam behaviour for uni- and multiaxial tensile deformations is compared. To this end, four loading cases are considered: uniaxial tensile deformation in x_1- and x_2-direction, respectively, biaxial tensile deformation and triaxial tensile deformation. In case of the uniaxial tensile deformation in x_1-direction, the prescribed homogeneous strain field in the RVE is governed by the Green-Lagrange tensor $\boldsymbol{G} = \bar{\gamma}_{11}\boldsymbol{e}_1 \otimes \boldsymbol{e}_1$ with $0 \leq \bar{\gamma}_{11} \leq 2$. In Fig.4 the resulting stress-strain curves are presented. Regarding the uniaxial tensile deformation in x_1-direction as shown in Fig. 4(a), equal normal stresses in the 2D model foam develop in the small strain regime. However, with increasing macroscopic strain, anisotropy is induced in the initially isotropic 2D-microstructure due to the alignment of the struts in the loading direction. This effect is reflected by the different material's response normal to the loading direction (compare (a) with (b)). Whereas the normal stress components in the macroscopic loading direction are approximately equal, independently whether the foam is elongated in the x_1-direction or in the x_2-direction, the out of plane stresses perpendicular to the loading direction are significantly different. A similar effect can also be observed for the 3D model foam according to Fig. 4(a) and (b), respectively.

As a next example, both model foams are compared for biaxial loading. Since the cell walls of the 2D model foam are only elongated, no deformation induced anisotropy occurs in this case. From the point of view of the meso-deformation mechanisms, the biaxial loading of the 2D model foam is rather comparable with the triaxial tensile loading of the Kelvin foam. As a result, a hydrostatic state of stress is induced in the 3D model foam (see Fig. 4(d)).

As a conclusion of the tensile loading simulations, it is found that the 3D-model appears to be comparatively softer within the small strain domain than the 2D model foam. However, the stress-strain curves of the 2D model are qualitatively similar due to the same meso-deformation mechanisms like localized bending and cell wall stretching. Distinct differences occur only in the stress level.

4.2. Shear deformation

Another basic loading case is the pure macroscopic shear deformation $\boldsymbol{G} = \bar{\gamma}_{12}\boldsymbol{e}_1 \otimes \boldsymbol{e}_2 + \bar{\gamma}_{21}\boldsymbol{e}_2 \otimes \boldsymbol{e}_1$ in the x_1, x_2-plane with $\bar{\gamma}_{12} = \bar{\gamma}_{21}$. In Fig. 5 the effective

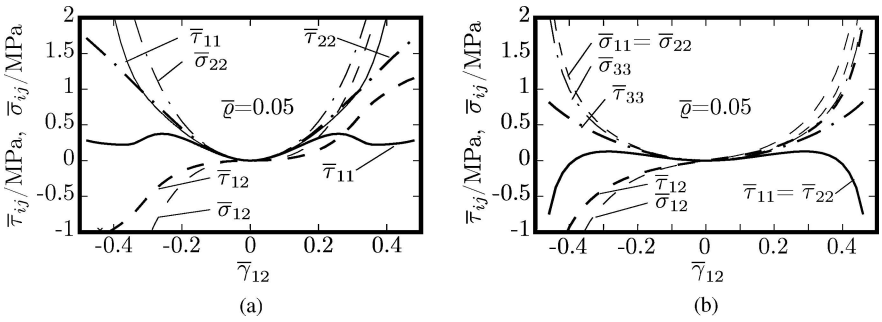

Figure 5 Effective stress-strain behavior under shear deformation for (a) the 2D model foam and (b) the 3D model foam.

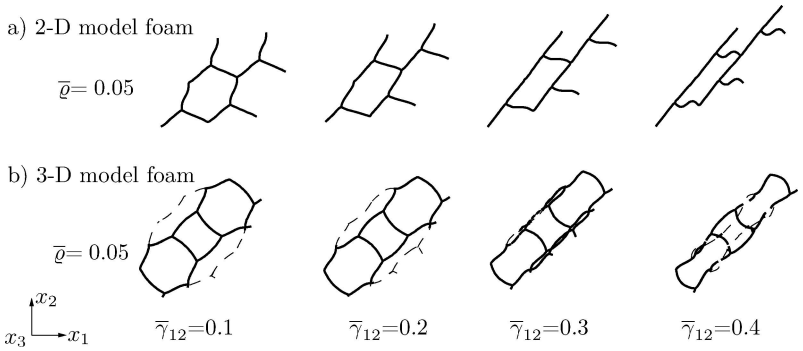

Figure 6 Morphology change of the 2-D and 3-D model foam under pure shear deformation.

stress-strain curves for both model foams are plotted. On the one hand, there is a distinct difference between the foam behaviour at small and large effective strains. In the small strain regime only shear stresses develop in the 2D and 3D-microstructure, whereas at large effective strains relatively high effective normal stresses are induced additionally due to stretching of the cells on the meso scale. On the other hand, the material responses of both microstructures are qualitatively similar.

In Fig. 6 the morphology change of both microstructures related to the stress strain curves can be observed. At macroscopic strains $\bar{\gamma}_{12} \approx \pm 0.3$, the normal stress-strain curve for $\bar{\tau}_{11}$ shows a local maximum since the struts loaded in compression start to buckle. Also, both microstructures again exhibit deformation induced anisotropy since the symmetry of both microstructures gets lost and the cells are reorientated according to the shear loading. Besides the 2nd Piola-Kirchhoff stresses, the corresponding Cauchy stress are plotted (see Equation 5).

4.3. Uni- and multiaxial compressive deformation

The response of both microstructures subjected to uniaxial compressive deformation is shown in Fig. 7. Due to the fact that the critical buckling loads of the 3-D model are about 10times higher than the buckling loads of the 2-D model foam, the corresponding stress-strain curves develop at different stress levels. Nevertheless, the stress-strains can be regarded as typical for open-cell foams. The stress-strain curve consists of a small strain regime where the stress-strain curve is nearly linear, followed by a stress plateau and a densification regime. Note that no cell wall contact has been taken into account. The steep increase of the stress is due to the employed stress and strain measure. Comparable with the uniaxial tensile deformation, a deformation induced anisotropy effect can also be observed at high compressive strains. After bifurcation decreasing normal stresses develop perpendicular to the loading direction. In addition, the cubic symmetry of the undeformed 3-D microstructure vanishes. With regard to the meso-deformations, the 3-D model foam shows localized bending and buckling effects which are similar to the 2-D material behaviour. Thus, the resulting effective stress-strain curves of both microstructures agree closely in a qualitative manner.

In Fig. 8(a) the biaxial stress-strain response is shown which differs from the uniaxial stress-strain curves in the slope of the stress-plateau. While equal normal second Piola-Kirchhoff stresses $\bar{\tau}_{11}$ and $\bar{\tau}_{22}$ develop in the 2-D microstructure, only the normal stresses in x_1- and x_2-direction coincide in the 3D-case. The 3-D model foam exhibits a softening effect in the stress component $\bar{\tau}_{33}$ after bifurcation.

A completely different stress-strain behaviour is observed for the 3-D model foam subject to triaxial compressive deformation (see Fig. 8b). First, bifurcation buckling occurs followed by snap-through buckling. With onset of bifurcation the equivalence of the normal stresses are preserved up to effective strains of $\bar{\gamma}_{11} > -0.1$. In contrast to bifurcation buckling, the stress-strain curve $-\bar{\tau}_{11}$ has a local extremum and then exhibits a negative stiffness for snap-through buckling. Consequently, the model foam has to release strain energy in order to achieve static equilibrium resulting in instability failure of the microstructure.

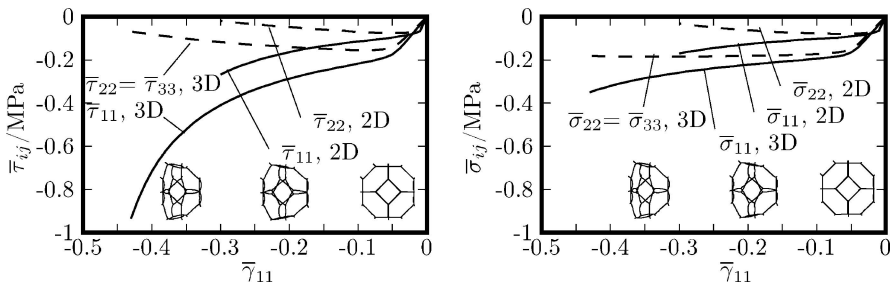

Figure 7 Post-buckling behavior of the 3-D model foam under uniaxial compression.

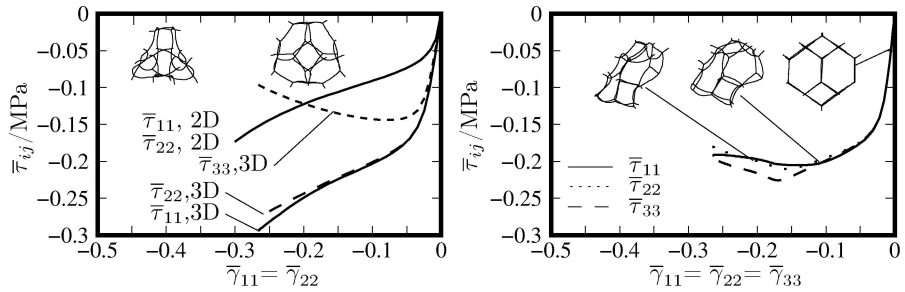

Figure 8 Post-buckling behavior of the 3-D model foam under (a) biaxial and (b) triaxial compression.

5. Conclusions

The main goal of this contribution is to study the effect of different modeling dimensions on the overall mechanical properties of open-cell foams. To this end, highly idealized models consisting of a hexagonal microstructure and the Kelvin-foam are adopted. The material response to basic loading cases is compared using a strain energy based homogenisation scheme. The basic assumption within this homogenization approach is to derive the effective stress-strain relationships by volume averaging of the elastic strain energy.

From the numerical examples for uniaxial tensile deformation we can conclude that both foam models have a similar qualitative stress-strain behaviour. Therefore, neglecting the spatial morphology results only in different stress levels of the macroscopic stress-strain curves since on the meso scale the same deformation mechanism are observed. In addition, both model foams show the effect of deformation induced anisotropy which is caused by the morphology change at large macroscopic strains. In case of uniaxial compressive loading, a typical stress-strain curve for foamed materials is obtained. However, it is emphasized that the obtained results cannot be generalized simply to real honeycombs and foams because of the idealized geometry and the particular assumptions. The existing distinctions in their overall behaviour are rather supposed to emerge more pronounced.

Acknowledgements

The financial support by the German Research Foundation (DFG) under grand no. KR1999/4-1 and BE1090/12-1 is gratefully acknowledged.

References

1 A. GENT and A. THOMAS, Mechanics of foamed elastic materials. *Rubb. Chem. Techn.* **36** (1963) 597.
2 M. PATEL and I. FINNIE, Structural features and mechanical properties of rigid cellular plastics. *J. Mater.* **5** (1970) 909.
3 L. GIBSON and M. ASHBY, Cellular Structures and Properties (Cambridge University Press, 2nd edn. 1997).
4 W. E. WARREN and A. M. KRAYNIK, Foam mechanics: The linear elastic response of two-dimensional spatially periodic cellular materials, *Mech. Mater.* **6** (1987) 27.
5 S. LEKHNITSKII, Theory of Elasticity of an Anisotropic Elastic Body. (Holden-Day, San Francisco, 1963).
6 W. E. WARREN and A. M. KRAYNIK, Linear elastic behavior of a low-density {K}elvin foam with open cell, *J. Appl. Mech.* **64** (1997) 787.
7 H. ZHU, J. F. KNOTT and N. J. MILLS, 'Analysis of the elastic properties of open-cell foams with tetrakaidecahedral cells, *J. Mech. Phys. Solids* **45**(3) (1997a) 319.
8 L. GRENESTEDT, Effective elastic behaviour of some models for 'perfect' cellular solids, *Intern. J. Solids Struct.* **36**(10) (1999) 1471.
9 A. DEMENTJEW and O. TARAKANOV, Effect of cellular plastics by the finite element method. *Poly. Mech.* **6** (1970) 519.
10 H. X. ZHU, N. J. MILLS and J. F. KNOTT, Analysis of the high strain compression of open-cell foams, *J. Mech. Phys. Solids* **45**(11–12) (1997b) 1875.
11 Y. WANG and A. M. CUITIÑO, Three-dimensional nonlinear open-cell foams, *J. Mech. Phys. Solids* **48** (2000) 961.
12 H. X. ZHU, J. R. HOBDELL and A. H. WINDLE, Effects of cell irregularity on the elastic properties of open-cell foams, *Acta Mater.* **48** (2000) 4893.
13 R. HILL, Elastic properties of reinforced solids: Some theoretical principles. *J. Mech. Phys. Solids* **11** (1963) 357.
14 J. HOHE and W. BECKER, Effective mechanical behavior of hyperelastic honeycombs and two-dimensional model foams at finite strain. *Intern. J. Mech. Sci.* **45** (2003) 891.

Received December 2004
and accepted April 2005